CrossMark

ORIGINAL ARTICLE

Differential frequency-dependent antidromic resonance of the Schaffer collaterals and mossy fibers

Luis M. Franco · Jesús Q. Beltrán · Jesús A. Tapia ·
Franco Ortiz · Elías Manjarrez · Rafael Gutiérrez

Abstract To better understand information transfer along the hippocampal pathways and its plasticity, here we studied the antidromic responses of the dentate gyrus (DG) and CA3 to activation of the mossy fibers and Schaffer collaterals, respectively, in hippocampal slices from naïve and epileptic rats. We applied trains of 600 electrical stimuli at functionally meaningful frequencies (θ, β/γ and γ). The responses of the DG to θ frequency trains underwent rapid potentiation that lasted about 400 stimuli, after which they progressively returned to control value. At β/γ and γ frequencies, however, the initial potentiation was followed by a strong frequency-dependent depression within the first 50 stimuli. In kindled animals, the initial potentiation was stronger than in control preparations and the resonant phase at θ frequency lasted longer. In contrast, CA3 responses were exponentially depressed at all frequencies, but depression was significantly less intense at θ frequency in epileptic preparations. Failure of fibers to fire

action potentials could account for some of the aforementioned characteristics, but waveforms of the intracellular action potentials also changed as the field responses did, i.e., half-duration and time-to-peak increased in both structures along the stimulation trains. Noteworthy, block of glutamate and GABA ionotropic receptors prevented resonance and reduced the depression of antidromic responses to β/γ and γ stimulation recorded in the DG, but not in CA3. We show that the different behavior in the information transfer along these pathways depends on the frequency at which action potentials are generated, excitability history and anatomical features, including myelination and tortuosity. In addition, the mossy fibers are endowed with ionotropic receptors and terminal active properties conferring them their sui generis non-passive antidromic responses.

L. M. Franco · J. Q. Beltrán
Department of Physiology, Biophysics and Neurosciences, Centro de Investigación y Estudios Avanzados del Instituto Politécnico Nacional, Av. Instituto Politécnico Nacional, 07360 Mexico D.F., Mexico

J. A. Tapia · E. Manjarrez
Institute of Physiology, Benemérita Universidad Autónoma de Puebla, 14 Sur 6301, 72570 Puebla, Mexico

F. Ortiz · R. Gutiérrez (✉)
Department of Pharmacobiology, Centro de Investigación y Estudios Avanzados del Instituto Politécnico Nacional, Calzada de los Tenorios No. 235, 14330 Mexico D.F., Mexico
e-mail: rafagut@cinvestav.mx

F. Ortiz
Institute of Cell Physiology, Universidad Nacional Autónoma de México, Ciudad Universitaria, Mexico D.F., Mexico

Introduction

The output of information from the dentate gyrus (DG) via its mossy fibers (MFs), its integration by the pyramidal cells of CA3 and, in turn, their output of information via the Schaffer collaterals (SCs) to CA1 must be tuned to allow an efficient passage of information along the hippocampal circuit (Jaffe and Gutiérrez 2007). How this is achieved is poorly understood. In hippocampal slices recorded in an air-to-liquid interface chamber under normal artificial cerebrospinal fluid (ACSF), CA3 displays endogenous θ and β/γ rhythmic activity, whereby the latter is primarily sustained by a GABAergic circuit (Treviño et al.

2007; Pietersen et al. 2009). When MFs are activated at β/γ frequency, EPSP–spike coupling in pyramidal cells of CA3 seems to be better than at lower or higher frequencies (Treviño et al. 2007, 2011), suggesting a resonance phenomenon. The underlying cause of this apparent resonance can be explained by either a better transfer capacity of the MF at this frequency range or by a proneness of CA3 cells to better follow such frequency. To address this, we studied the capacity of CA3 and DG to respond to antidromic activation of the SCs and MFs, respectively, at different frequencies: 5, 10, 24 and 40 Hz, which, constitute functionally relevant rhythms (δ, θ, β/γ and γ) in the hippocampus. To analyze antidromic responses recorded in CA3 and the DG, we directly stimulated the SCs and MFs, respectively, in the presence and absence of antagonists of glutamate and GABA ionotropic receptors. In a set of experiments, we also compared recordings from the fiber tracts themselves and from the pyramidal and granular cell layers of CA3 and DG. Neuronal assemblies must have specific characteristics as defined from their distinctive architecture, and their transmission capacities may be affected by their differences in myelination as well (Meier et al. 2004; Alle et al. 2009). Therefore, in this work we ask: Which information transfer properties underlie the functional coupling of the DG—or the mossy fibers—with CA3, and from there—Schaffer collaterals—to CA1? Do their known different myelination, channel and receptor distribution, as well as their morphological characteristics affect action potential conduction to the soma? Can kindling epilepsy modify any of the aforementioned characteristics?

Our results show that the morphological and electrical properties of the major conduction pathways in the hippocampus differ in the kinetics in which they conduct repetitive antidromic potentials. This suggests that a counterbalanced activity-dependent mechanism can potentiate the transfer of information at a preferred or optimal frequency, namely at the θ frequency range.

Materials and methods

Electrophysiological recordings

The Ethics Committee for Animal Research at our institution approved all experimental procedures. For our recordings, we used acutely prepared combined entorhinal cortex–hippocampus slices (400 µm). They were obtained from young adult (5 weeks of age) naïve and electrically kindled (8 weeks of age) Wistar rats, the day on which the 5th stage V seizure was induced, as previously described (Gutiérrez 2000). Slices were kept in oxygenated artificial cerebrospinal fluid (ACSF) at room temperature at least for

1 h before they were transferred to the recording chamber. For recording, the slices were transferred to an air–liquid interface chamber and were constantly perfused (1 ml min^{-1}) with oxygenated ACSF at 34 ± 0.5 °C containing (in mM): NaCl, 124; KCl, 3 and 5 (see "Results"); NaH$_2$PO$_4$, 1.25; MgSO$_4$, 2; CaCl$_2$, 2 and 1.2; NaHCO$_3$, 26, and glucose, 10; pH 7.35. The drugs used were diluted in the ACSF, namely the NMDA receptor antagonist (D, L)-2-amino-5-phosphonovaleric acid (APV; 30 µM; Tocris-Cookson, Ellisville, Missouri); the non-NMDA receptor antagonist 6-nitro-7-sulfamoylbenzo-(f)quinolaxine-2,3-dione (NBQX; 10 µM; Tocris-Cookson); the GABA$_A$ receptor antagonists picrotoxin (100 µM; Sigma-Aldrich) and gabazine (10 µM; Sigma-Aldrich). Antidromic, extracellular field potentials were recorded with glass microelectrodes (5–10 MΩ) filled with NaCl (155 mM) placed over the pyramidal cell layer of CA3 area and over the granular cell layer of the DG (Fig. 1a$_1$, a$_2$). A second series of extracellular recordings (see "Results") were conducted on the stratum lucidum, to record the antidromic population action potential ($_f$AP) traveling along the MFs, and on the stratum oriens of CA3, to record the antidromic $_f$AP evoked in the SCs. Intracellular recordings were conducted with borosilicate microelectrodes (65–75 MΩ) filled with 2 M potassium acetate (Sigma-Aldrich). Electrophysiologically identified pyramidal cells were recorded from regions CA3a and b, and granule cells were recorded from the upper blade of the DG. Both intra- and extracellular signals were acquired using an AxoClamp 2B amplifier (Molecular Devices, Foster City, CA). Signals were digitized (at 10 kHz; Digidata, Molecular Devices) and acquired with the pClamp 9 Software (Molecular Devices). Stimulation to the SCs and to the MFs (Fig. 1a$_1$, b$_1$) was provided with a Grass S11 stimulator through a photoelectric stimulus isolating unit (PSIU 6; Grass Instr. Co.) connected to a bipolar (tip separation 50 µm), glass-insulated platinum wire (25 µm) electrode. We delivered 4 trains of 600 pulses of 0.1 ms, each at 5, 10, 24 and 40 Hz with an intertrain interval of 2 min, under control ACSF perfusion, after which the blockers were perfused to record the same type of responses during the block of glutamate and GABA$_A$ receptors (see Fig. 1). The current intensity, at which the trains were delivered, was determined for each experiment with an input–output curve, whereby the minimal stimulation needed to evoke antidromic $_f$APs was used to assess $_f$AP failures and kinetics changes.

Data analysis

We measured the peak latency, the amplitude and the duration of the field antidromic responses, as well as of the intracellular responses evoked under each experimental condition (Fig. 1a; see "Results") using the built-in

Fig. 1 Schematic representation of the experimental setup and results obtained in control slices. Antidromic field action potentials were evoked in the DG by stimulation of the MFs (**a₁**) and in CA3, by stimulation of the SCs (**b₁**) at 5, 10, 24 and 40 Hz. **a₂** Long time scale and short time scale sample traces of the antidromic field potentials evoked in the DG and in CA3 (**b₂**; $n = 6$ for each region). All stimulus artifacts were suppressed. We measured the amplitude, peak latency and half-duration of each antidromic field action potential in the trains. *Calibration bars* in (**b₂**) also apply to (**a₂**). **c**, **d** Plots of the normalized responses along the train for each frequency and pharmacological condition. **c** Stimulation at slow and fast θ frequencies of the MFs provoked an initial potentiation followed by a long plateau of potentiated responses (resonance; *vertical black dotted line*). The *vertical red dotted lines* signal the stimulus in the 10 Hz train at which the amplitude returned to the value of the first response. **d** Stimulation of the SC provoked a frequency-dependent exponential depression in CA3. The *vertical black dotted lines* indicate the plateau values
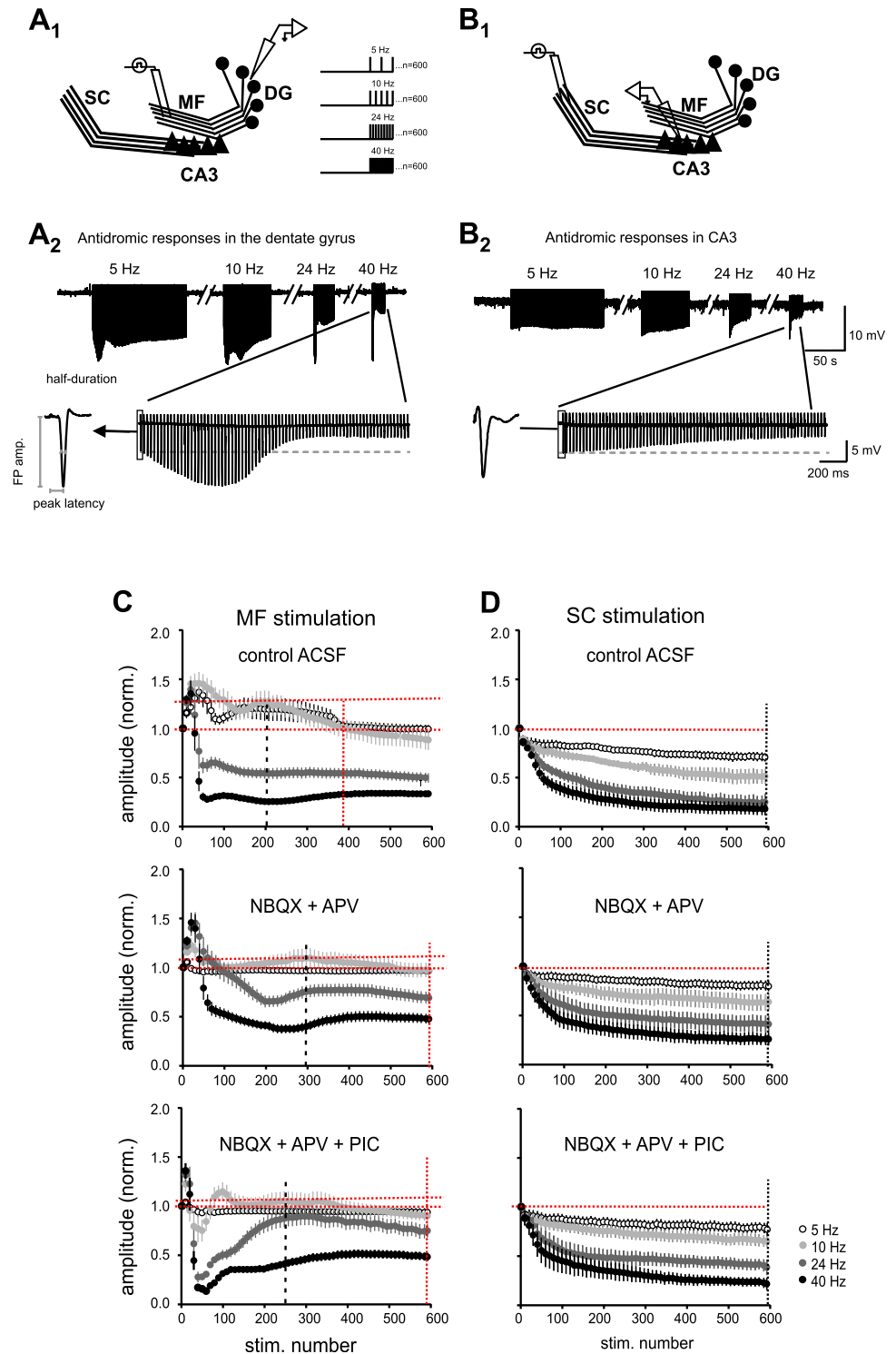
functions of pClamp 10. The onset latency of the responses was measured from the beginning of the stimulation artifact to the first inflection point of the first derivative of the signal. For our analysis of resonance (Figs. 1, 2, 3), the amplitude of all the extracellular antidromic responses in DG and CA3 was normalized using the responses of the DG to 5 Hz stimulation, in the presence of glutamate and GABA receptors antagonists, as reference for normalization. A similar normalization procedure has been employed in other studies about resonance (Manjarrez et al. 2003). We considered that "antidromic resonance" occurred when the amplitude of the antidromic field responses

Fig. 2 Results obtained in slices from epileptic rats. **a** Mossy fiber stimulation at θ frequency provoked potentiation of the responses in the DG, which was stronger and followed by a longer plateau (resonance; *vertical black dotted line*) than responses recorded in control preparations (see Fig. 1). Perfusion of glutamatergic (NBQX+APV) and GABAergic blockers (+PIC) inhibited the potentiation provoked by θ frequency stimulation. The *vertical red dotted lines* signal the stimulus in the 10 Hz train at which the amplitude returned to the value of the first response. **b** Stimulation of the SC at 5, 10, 24 and 40 Hz provoked an exponential inhibition of the responses recorded in CA3. The *vertical black dotted line* indicates the stimulus number at which the plateau value was obtained. The *vertical red dotted lines* indicate the plateau value
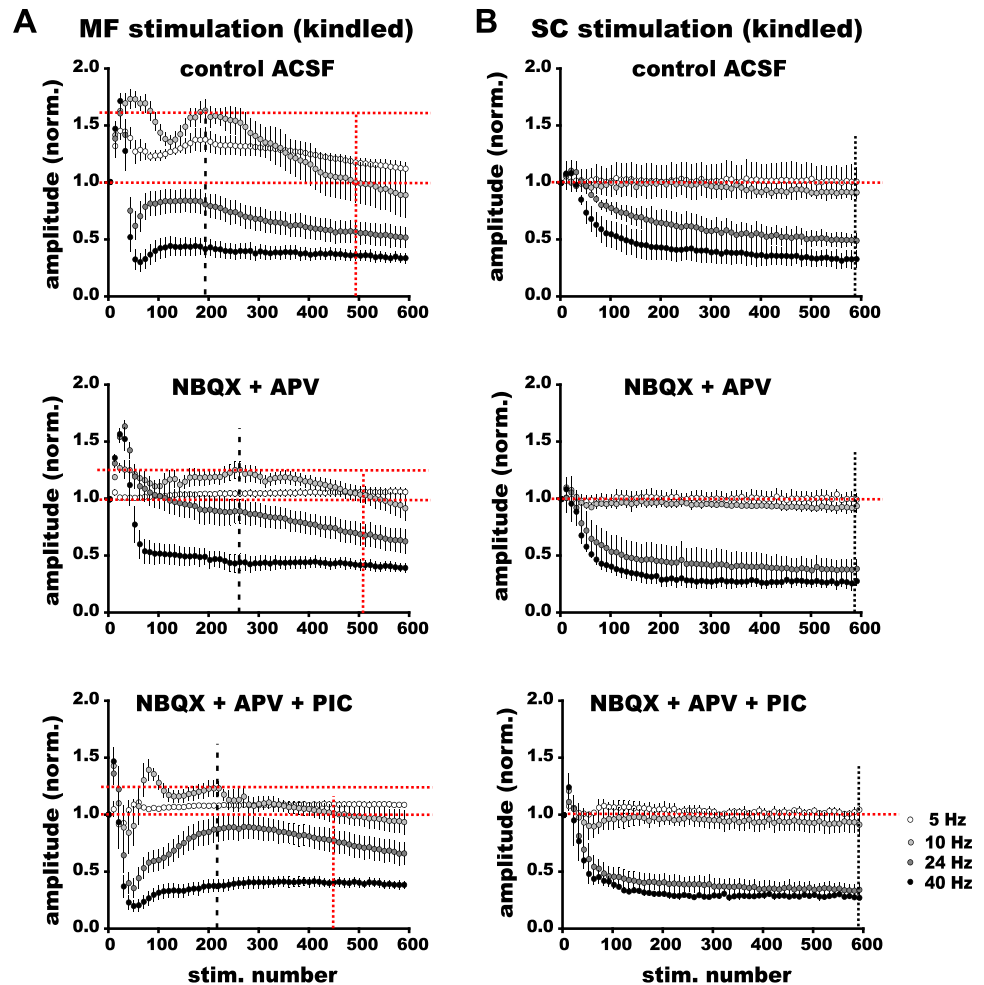
significantly increased with respect to the first evoked potential in these conditions. Also, to better represent changes in amplitude and half-width of the intracellularly recorded action potentials along the stimulation trains, they were normalized as well (Figs. 7, 8). Units of measurement for each plot are clarified in the corresponding legends. To determine the statistically significant difference between groups (control vs kindled) and conditions (frequencies and pharmacologic) we performed a Student's t test for pooled independent samples. Also, we performed a one-way ANOVA to compare the amplitude of the $_f$APs obtained at different pharmacological conditions for a given antidromic stimulation frequency.

Histological procedure

To label the SCs as well as the MFs, we introduced a small crystal of fluorescein–dextranamine (Molecular Probes, Eugene, OR) in the granular cell layer of the DG or in the pyramidal layer of CA3 with the aid of a micropipette tip (Boulton et al. 1992). The dye is taken up into the neurons

and anterogradely and retrogradely transported along the axons. Because we focused in the anterogradely labeling of the axons that constitute the MFs and Schaffer collaterals, we kept the slices in an air–liquid interface chamber, constantly perfused with oxygenated storage solution at room temperature for 3–4 h after introducing the crystal. Photomicrographs were obtained with a confocal microscope Leica TCS SP2. Digitized images were processed with the Leica Application Suite Advanced Fluorescence Lite (LAS AF Lite, Ver. 2.6.0).

Results

We first determined the effect of different frequencies of stimulation on the amplitude, half-duration, and peak latency of the antidromic field responses of the DG ($n = 6$) and of CA3 ($n = 6$) evoked by stimulation of MFs (Fig. 1a$_1$, a$_2$) and SCs (Fig. 1b$_1$, b$_2$), respectively. These parameters were measured for each antidromic response along the stimulation trains of different frequencies and in
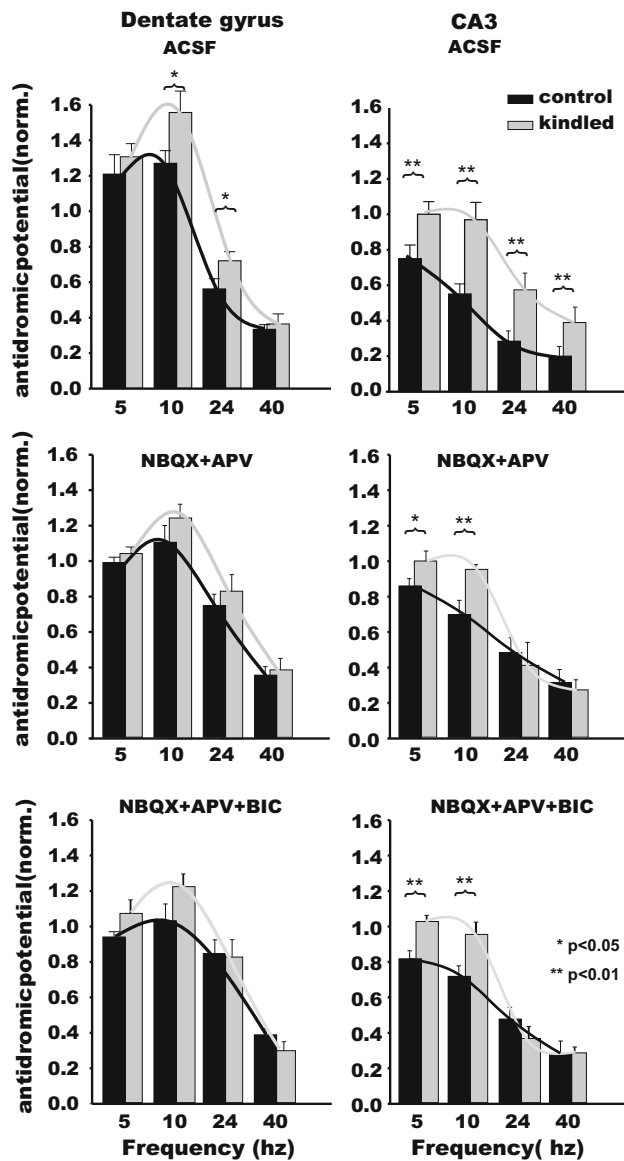
Fig. 3 Summary of the normalized antidromic responses of Figs. 1 and 2, obtained when the responses reached a plateau value in the three pharmacological conditions ACSF, NBQX + APV, and NBQX+APV+BIC. The amplitude of all the antidromic responses in DG and CA3 was normalized using the antidromic responses of the DG to 5 Hz stimulation in the presence of glutamate and GABA receptors antagonists, as reference for normalization (*black bar* at 5 Hz in the last graph of DG). The *left panel* shows that the amplitude of the antidromic responses exhibited a resonance at 5 and 10 Hz in control ACSF in control rats (see how the *black bars* in ACSF conditions exhibit a significant increase relative to 1). Such DG antidromic resonance occurred for 5 and 10 Hz (slow and fast θ) but not for the β/γ and γ frequencies in both control, and kindled rats; therefore, antidromic resonance is frequency dependent. CA3 did not exhibit antidromic resonance for control rats (*black bars*) but kindled rats (*gray bars*) exhibited an antidromic resonance for 5 ($p \leq 0.05$) and 10 Hz ($p \leq 0.01$) even in the presence of NBQX + APV, and NBQX + APV + BIC

the different pharmacological conditions (Fig. 1c, d): in control ACSF, during blockage of ionotropic glutamate receptors with NBQX (10 μM) and APV (30 μM), and during additional blockade of phasic and tonic $GABA_A$ receptors with picrotoxin (100 μM) or gabazine (10 μM). Figure $1a_2$, b_2 depicts sample traces of the antidromic potentials evoked in the DG and CA3, respectively, by the different stimulation frequencies (5, 10, 24 and 40 Hz).

The normalized amplitudes of the antidromic responses evoked by high-frequency stimulation are depicted in group plots in Fig. 1c, d. In brief, high-frequency stimulation of the MFs at 5 and 10 Hz in normal ACSF initially provoked a potentiation of the responses (121 and 127 %, respectively), peaking by the 30th response, after which they remained potentiated (see Fig. 3) for the next 360 stimuli and returned to control values after 400 stimuli. This frequency specificity of the long-duration resonance was only observed at 5 and 10 Hz (see Fig. 3). In contrast, when the stimuli were delivered at 24 and 40 Hz, the responses were initially potentiated to 145 % by the 21–24th stimulus, after which a fast depression (24 Hz, 56 %; 40 Hz, 34 % of the control value) was observed for the remaining of the trains (Fig. 1c). In clear contrast, CA3 responses presented a different trend, whereby responses were exponentially depressed along the train in a frequency-dependent manner, reaching 20 % of the control responses at 40 Hz (Fig. 1d). Perfusion of glutamate blockers depressed the initial potentiation of the responses of the DG to 5 and 10 Hz stimulation but not to 24 and 40 Hz stimulation. However, in the latter, the depression provoked after the initial potentiation was less pronounced. Interestingly, the addition of the $GABA_A$ receptor blocker, picrotoxin (100 μM), provoked a steeper and stronger depression (>75 %) after the initial potentiation (Fig. 1c). By contrast, the response to high-frequency stimulation of the SCs was not affected by perfusion of the antagonists (Fig. 1d). We additionally conducted control experiments in which we used gabazine (10 μM; $n = 6$) instead of picrotoxin as GABA-R blocker, and found no difference in the results from both sets of experiments (not shown).

We next conducted the same series of experiments in slices obtained from kindled epileptic rats. Figure 2a shows a response trend, similar to that observed in the control experiments. Interestingly, the initial potentiation provoked by stimulation at 5 and 10 Hz was more pronounced as well as the number of responses that remained above the values obtained in control slices (Fig. 2a). These higher values remained potentiated during a longer period of the stimulation train with respect to control slices (see Fig. 1). Responses of the DG during perfusion of glutamate and

GABA receptors' blockers did not differ significantly from control experiments. In summary, responses to 10 Hz underwent potentiation along the stimulus trains with the following characteristics: (1) the shift from potentiation to depression was significantly faster in control than in kindled preparations; (2) block of ionotropic glutamate receptors shortened the number of stimuli needed to shift potentiation to depression; (3) additional block of GABA phasic and tonic receptors produced a fast shift of the potentiated responses to depression. These changes were not observed in kindled rats, in which responses to 10 Hz remained potentiated for a longer time. Contrary to responses of CA3 from control rats, responses of slices from kindled rats underwent an initial potentiation for the first 30 responses, after which the exponential depression was observed. As described, the potentiation of the antidromic responses of the DG observed in the initial part of the stimulation train was followed by a plateau that had a distinctive duration in each experimental condition (control vs kindled; control vs glutamate and GABA-R block; and finally θ vs β frequency stimulation). Therefore, we took θ stimulation as a point of comparison to better analyze the effects of the different antagonists as well as of the kindled condition on the transmission fidelity of the pathways during the plateau. Figure 3 depicts the values of the antidromic responses at the peak of the plateau (vertical dashed lines in Figs. 1, 2), using the responses of the DG to 5 Hz stimulation in the presence of glutamate and GABA receptors antagonists as reference for normalization. Interestingly, antidromic stimulation at 10 and 24 Hz evoked responses in the DG of kindled preparations of higher amplitude with respect to those of control rats ($p < 0.05$). Under perfusion of glutamate and GABA antagonists, the responses were still higher at 5 and 10 Hz, although there was no significant statistical difference between both groups. By contrast, antidromic responses of CA3, which were exponentially depressed in all conditions, were less depressed in kindled epileptic preparations under control ACSF perfusion for all stimulation frequencies. However, when the stimulation was provided in the presence of glutamatergic antagonists, only the θ band (5 and 10 Hz) was significantly higher in the kindled group with respect to control preparations. This difference did not change by addition of the GABAergic antagonists.

Repetitive antidromic stimulation produced a progressive widening of the antidromic $_fAP$ along the train. Figure 4a$_1$ depicts representative responses of the DG to MF stimulation, which were superimposed using the peak value as reference to observe the change of amplitude and duration during a 24-Hz stimulation train. Figure 4a$_2$ shows representative responses of the DG time-locked in the stimulus artifact to observe how the peak latency shifts along the 24-Hz stimulation train. Figure 4c$_1$, c$_2$ illustrates

representative responses of CA3 to SC stimulation during a 24-Hz stimulation train. Figure 4b$_1$ shows the trend of the $_fAP$ width changes in the DG, which reached approximately 120 % of the half-duration of the first response at 5 and 10 Hz, and 170 % at 24 and 40 Hz. These parameters were not modified when ionotropic glutamate and GABA$_A$ receptors were blocked. The latency to the peak of the responses was also shifted along the train from 1.1 ms at 5 Hz to 1.6 ms at 40 Hz, in a frequency-dependent manner (Fig. 4b$_2$). Also, these parameters were not modified by the blockage of ionotropic glutamate and GABA receptors. The antidromic $_fAPs$ of CA3 underwent a widening as the stimulus train progressed to 198 % at 40 Hz (Fig. 4d$_1$). The latency to the peak also shifted from 1.2 to around 2.2 ms as the stimulation train progressed (Fig. 4d$_2$). Interestingly, although blocking glutamate and GABA$_A$ receptor antagonists did not change the magnitude of the effects, it reduced the variability of the responses to high-frequency stimulation. The half-width duration and peak latency of the antidromic responses were also measured in hippocampal slices of kindled epileptic rats. As shown in Fig. 5, no clear difference was observed when compared with control animals. However, it is noteworthy that the values of these parameters measured in CA3 had a higher variability in kindled vs control preparations.

Because the depression of the $_fAPs$ along the stimulation trains may be explained by the failure of the fibers to conduct action potentials, we conducted intracellular recordings in CA3 and in the DG while stimulating the SCs and MFs, respectively. Furthermore, because of the similarity of the responses of control and kindled rats, and as proof of principle, we only conducted these experiments on slices of control rats. As expected, the stimulation trains delivered to the SCs and MFs failed to trigger action potentials in a frequency-dependent manner both, in pyramidal ($n = 5$) and granular cells ($n = 5$), respectively. Figure 6 depicts an example of intracellularly recorded responses of a pyramidal cell to MF stimulation.

We next analyzed the kinetics of the intracellularly recorded antidromic action potentials. To this end, we raised the stimulus intensity to evoke action potentials for every stimulus of the train, and measured the amplitude, half-width, and time-to-peak of the intracellular responses, as well as the antidromic extracellular compound action potentials recorded over the MF and SC tracts (Figs. 7a$_1$, 8a$_1$). Note that, unlike the previous extracellular recordings made on the granular and pyramidal cell layers, the latter recorded the axonal volleys over the pathways themselves, i.e., without the participation of the somatic region (Figs. 7e–h, 8e–h). Again, to avoid contamination by conductances activated in the fibers by ambient glutamate and GABA, we conducted these experiments in the presence of ionotropic glutamate and GABA$_A$ receptor blockers. The change in

CONTROL RATS

DG antidromic field potentials
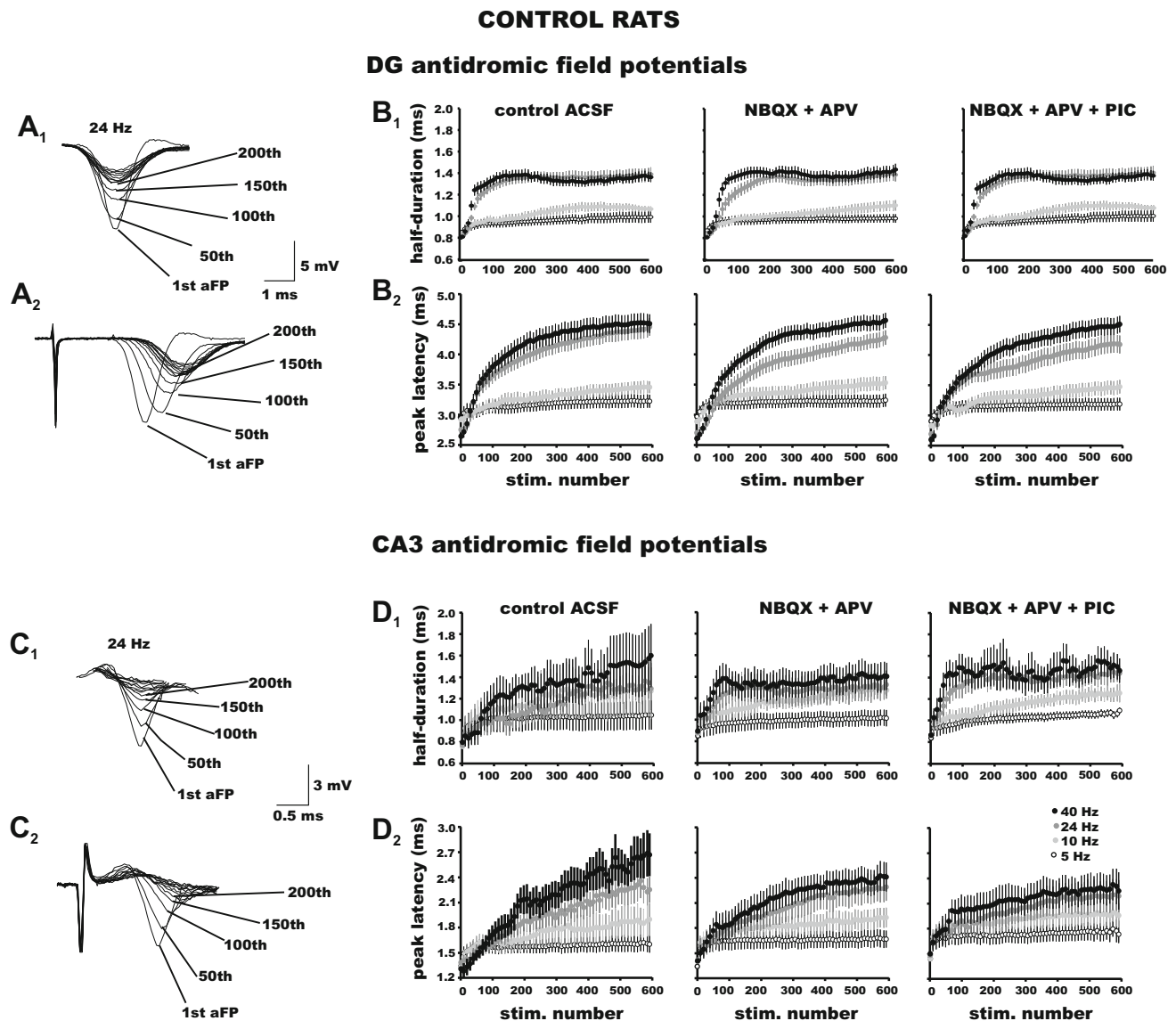

CA3 antidromic field potentials

Fig. 4 Characteristics of the antidromic potentials evoked in control preparations. Stimulus-dependent change in half-duration and peak latency of the antidromic field responses evoked in the DG by MF stimulation at 5, 10, 24 and 40 Hz. **a₁** Sample traces recorded in the DG showing the increase in half-duration of the antidromic field potential as the stimulus number increases within a train of 24 Hz. Traces are time-locked at the peak of the field potentials. **a₂** Sample traces showing the increase in peak latency of the antidromic field potential as the stimulus number increases within a train of 24 Hz.

Traces are time-locked at the stimulus artifact. **b₁** Plot of the half-duration of the antidromic field potential along the whole stimulus trains at the different stimulation frequencies. The half-duration increases progressively and in a frequency-dependent manner. **b₂** Plot of the peak latency of the antidromic field potential along the whole stimulus trains at the different stimulation frequencies. The peak latency increases progressively and in a frequency-dependent manner. Stimulus artifacts were suppressed. Panels (**c₁₋₂**) and (**d₁₋₂**), corresponding experiments conducted in CA3

amplitude of the intracellularly recorded APs, antidromically evoked by MF and SC stimulation at different frequencies, is depicted in Figs. 7b₁ and 8b₁. While the amplitude of the action potentials evoked in the granule cells was mildly depressed ($\sim 3\%$ mV) in a frequency-dependent manner (Fig. 8b₁), those evoked in the pyramidal cells underwent a stronger depression and presented a higher variability along the trains (~ 5–10%; Fig. 8b₁). These changes were accompanied by a mild hyperpolarization (3 mV) of

the membrane potential of the granule cells (Fig. 7b₂) and a stronger hyperpolarization of the pyramidal cells (6 mV; Fig. 8b₂). Interestingly, the extracellular responses of the MFs ($n = 5$; Fig. 7f₁), but not of the SCs ($n = 5$; Fig. 8f₁), underwent a transient potentiation of around 20 % at 24 and 40 Hz. These changes in MFs were accompanied by a change in the extracellular baseline potential (1 mV at 24 Hz; Fig. 7f₂), whereas this parameter did not change in the SCs recordings (Fig. 8f₂). Because high-frequency

Fig. 5 Characteristics of the antidromic potentials evoked in kindled preparations. **a** Plot of the half-duration of the antidromic field potentials evoked in the DG along the whole stimulus trains at the different stimulation frequencies. The half-duration increased in a frequency-dependent manner. Beneath, plot of the peak latency of the antidromic field potentials along the whole stimulus trains at the different stimulation frequencies. The peak latency also increased in a frequency-dependent manner. **b** Same measurements as (**a**), obtained in CA3
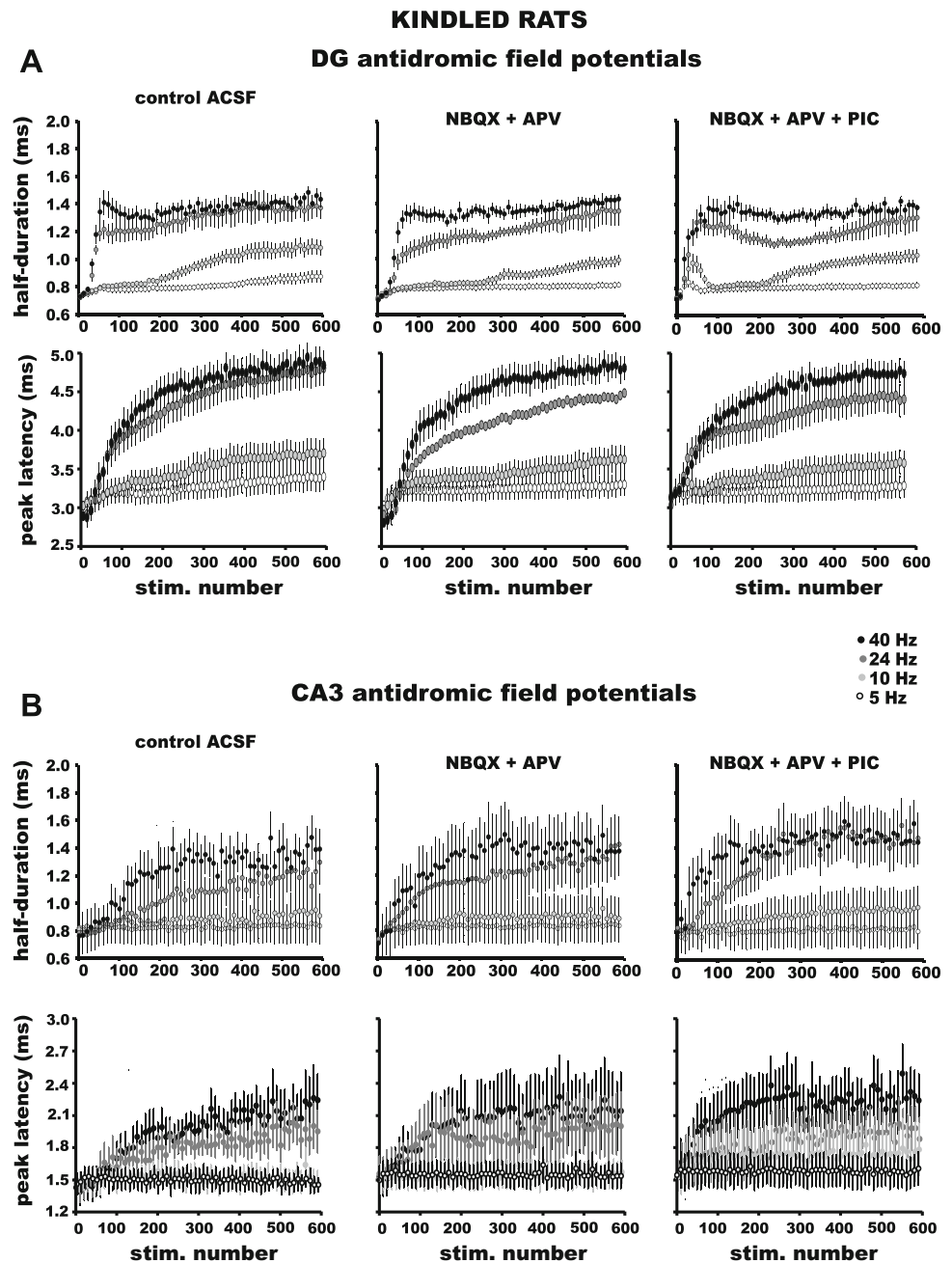

stimulation can provoke an extracellular accumulation of K^+, we conducted a series of experiments ($n = 6$) in which we used an ACSF containing 5 mM K^+ and 1.2 mM Ca^{2+} from the beginning of the recordings and in the presence of glutamate and GABA receptor blockers. Under this condition, single antidromic stimulation evoked $_fAPs$ that were variably potentiated by 30–50 % with respect to those obtained under normal ACSF perfusion, after which repetitive spontaneous spiking could be observed in CA3, but not in the DG. When high-frequency stimulation was applied, the trend of the amplitude of the responses along the trains of the

different frequencies was similar in the DG under control ACSF and under the presence of glutamatergic and GABAergic blockers. By contrast, comparing the responses along the stimulation trains obtained in CA3, but not in the DG, under control ACSF and those obtained in the high-K^+, low-Ca^{2+} ACSF, we did find a statistically significant inhibition of the responses at 10 Hz (31 % inhibition; $p < 0.005$), 24 (41 % inhibition; $p < 0.05$) and 40 Hz (32 % inhibition; $p < 0.001$).

We then analyzed the waveform of the intracellular action potentials along the trains. Figures $7c_1$, c_2 and $8c_1$,

Fig. 6 Intracellularly recorded antidromic action potentials in a pyramidal cell of CA3. Schaffer collaterals were stimulated with trains of different frequencies, at an intensity that provoked 60 % of the maximal field response in CA3. Note failures of action potentials at and above 10 Hz
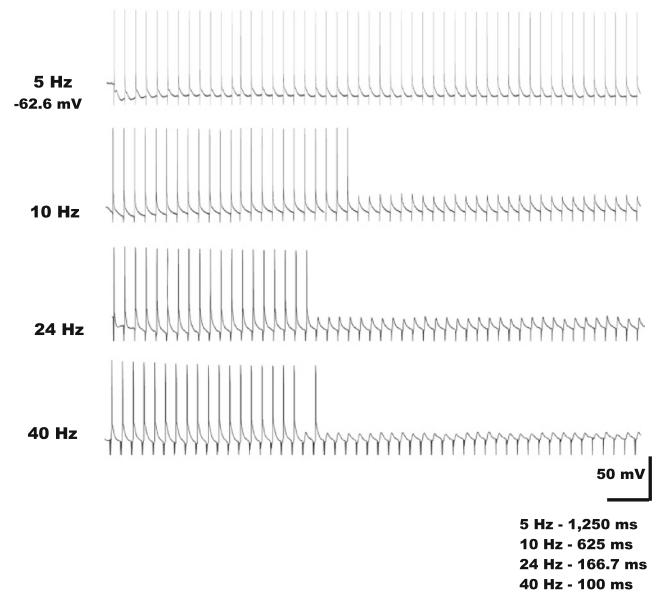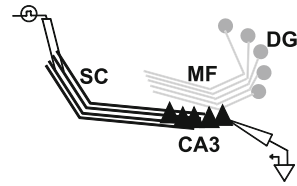
c_2 depict the change in half-width of the action potentials. In both cell types, the action potentials widened by 3–5 % at 5 and 10 Hz, and reached 12 % at 24 and 40 Hz. Again, the changes of the half-width of the action potentials of pyramidal cells presented a higher variability than that of the granule cells. Interestingly, as the train progressed, the intracellularly recorded antidromic APs of the granule cells presented a shoulder in the rising phase (Fig. 7c_1), which did not occur in the action potentials of the pyramidal cells (Fig. 8c_1). These effects paralleled the widening of the extracellular potentials. Finally, a similar shift to higher values was observed in the time-to-peak of the action potentials, both intra- and extracellularly recorded in both types of cells (Figs. 7 d_1, h_1, 8 d_1, h_1).

One of the possible explanations for the different responses observed in antidromic potentials evoked by MF and SC stimulation is, among others, the architecture and myelination of these pathways (see "Discussion"). To illustrate the morphology of the different pathways, we labeled them by introducing a crystal of dextranamine in the cellular region. Figure 9 depicts the difference of tortuosity and the presence of giant boutons and beads (boutons en passant) along the MFs, which are absent in the SCs. The MFs follow a narrow band along the stratum lucidum in CA3 while the SCs, although following a straight path to CA1, is broader and invades different regions of the apical dendrites of CA1 pyramids along the stratum radiatum.

Discussion

We previously showed that hippocampal slices, recorded in a liquid-to-air interface chamber, display a spontaneous θ

and β/γ oscillatory activity in CA3, and that the latter was reflected in interneuronal but not in pyramidal cell subthreshold membrane oscillations (Treviño et al. 2007). β/γ activity has also been observed in cholinergically induced oscillations in the hippocampus (Shimono et al. 2000) and in the somatosensory cortex in vitro (Roopun et al. 2006), while in vivo, an enhancement in the amplitude of β/γ oscillations was observed in CA3 during exploration of a novel environment (Berke et al. 2008).

Synaptic stimulation of CA3 pyramidal cells at the β/γ frequency range appeared to produce an enhanced EPSP–spike coupling as compared to lower and higher frequencies, and this suggested the existence of a synaptic resonance phenomenon (Treviño et al. 2007, 2011). The underlying cause of this apparent resonant activity can be either a better information transfer capacity of the MFs at this frequency, or by a proneness of CA3 cells to better integrate and follow such frequency. This work explores these possibilities. Interestingly, the granule cells normally fire at very low frequencies but can fire at high frequencies, in the β/γ range, in vivo (Jung and McNaughton 1993; Henze et al. 2002; Bower and Buckmaster 2008). In such cases, and during short periods, granule cells can consistently drive CA3 cells (Henze et al. 2002). Although it has been shown that the DG can entrain CA3 over a broad range of frequencies, the spontaneous oscillatory field activity of the DG peaks at 8 Hz (θ frequency), while in CA3 it peaks at 24 Hz (β/γ frequency; Treviño et al. 2007; Akam et al. 2012).

Our experiments using antidromic stimulation at functionally meaningful frequencies (θ, β/γ and γ) revealed some conduction/integration characteristics of the studied pathways that may bear physiological meaning in terms of

A₁ **Antidromic intracellular responses of GCs**

E₁ **Antidromic extracellular responses of MFs**
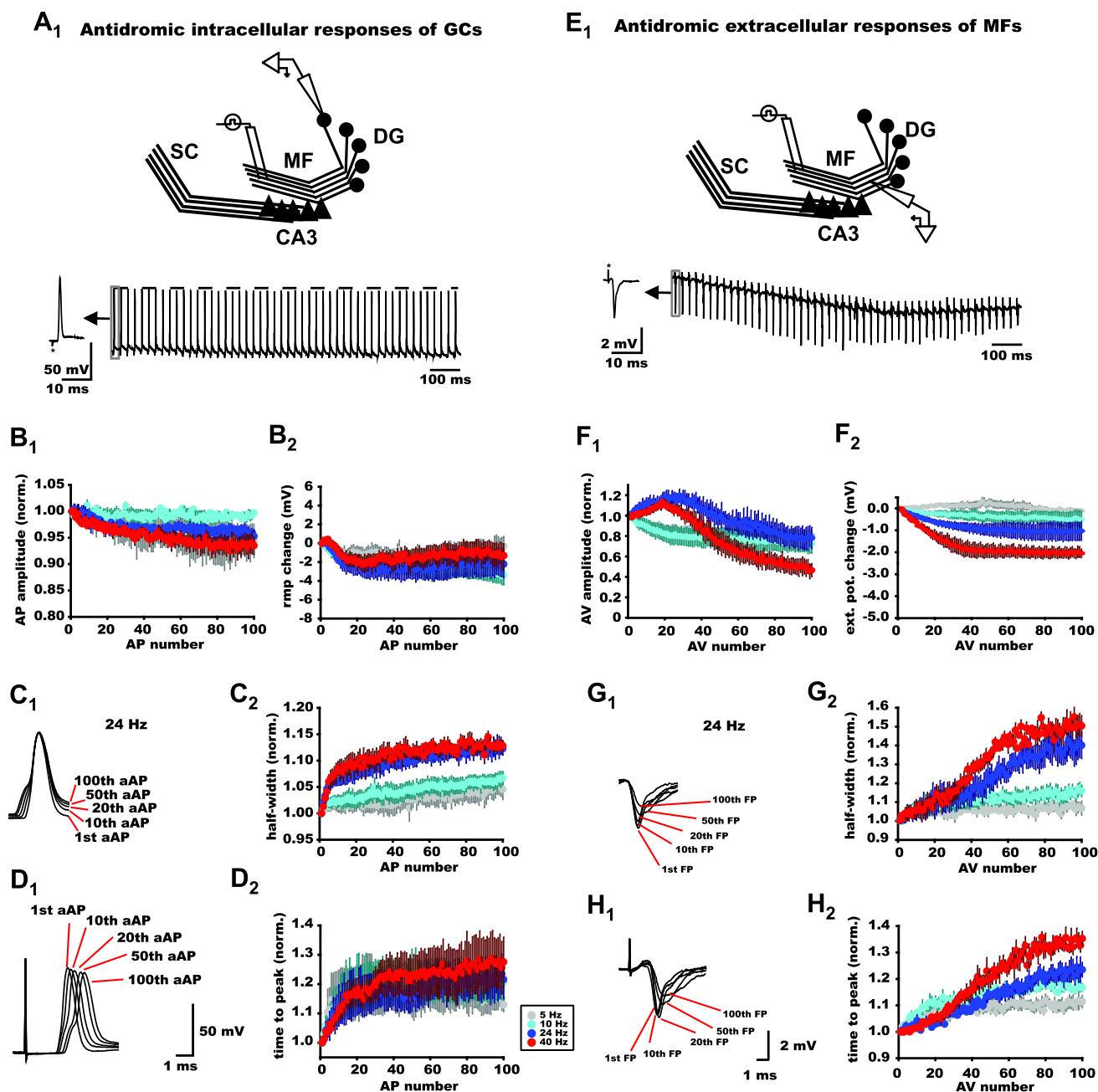
the coupling of activity of two substructures of the hippocampus: (1) MF stimulation produced an initial, rapid potentiation of antidromic responses in the DG followed by a plateau of lower magnitude, but still potentiated (maximal at 10 Hz under control ACSF). Thereafter, the responses were depressed in a frequency-dependent manner. Interestingly, block of glutamate and GABA receptors restricted the shift of the potentiated responses to depression. By contrast, SC stimulation produced a frequency-dependent exponential depression of CA3 antidromic responses in all the pharmacological conditions. Whereas MF stimulation in slices from epileptic rats also produced an

initial potentiation of the responses, they did not shift to depressed responses until after a large number of stimuli were delivered. In slices of kindled rats, SC stimulation at 5 and 10 Hz did not depress responses in the CA3 area; (2) In both structures, the $_f$APs broadened and their latency to the peak shifted to longer times as well. (3) We provided evidence that a possible failure of action potential generation as well as broadening of the field and intracellular APs seem to underlie this effect. In the DG, the increase in amplitude in the initial $_f$APs corresponded to an increase in the amplitude of intracellularly recorded action potentials in the granule cells, while there was a decrease in those of

◀ **Fig. 7** Behavior of antidromic potentials evoked by distal MF stimulation and recorded intracellularly in granule cells and extracellularly in MFs. a_1 Schematic representation of the experimental setup. Intracellular recordings were obtained from the granule cells and stimulation was provided at different frequencies over the MFs. Long time scale and fast time scale sample traces of intracellular recordings of a granule cell showing antidromic action potentials (AP, $n = 100$) on MF stimulation at 5, 10, 24 and 40 Hz. b_1 Plot of the amplitude of the antidromic APs along the train at the different stimulation frequencies. b_2 Plot of the RMP measured before each stimulus artifact along the stimulation train. c_1 Sample traces of the intracellular antidromic APs, time-locked at the peak; notice a broadening of the rising phase of the APs as stimuli progressed during a 24-Hz train. c_2 Plot of the APs half-width along the stimulation train, at the different stimulation frequencies. d_1 Sample traces of APs, time-locked at the stimulation artifact; notice an increasing delay of the AP onset as stimuli progressed during a 24-Hz train. *Calibration bars* apply to (c_1) and (d_1). d_2 Plot of the time-to-peak of the APs along the stimulation train at the different stimulation frequencies. e_1 Schematic representation of the experimental setup. Extracellular recordings were obtained from the MFs (stratum lucidum) and stimulation was provided at different frequencies over the terminal zone of the MFs. Long time scale and fast time scale sample traces of the extracellular recordings of stratum lucidum showing antidromic field action potentials (AP, $n = 100$) on MF stimulation at 5, 10, 24 and 40 Hz. f_1 Plot of the amplitude of the antidromic field action potentials along the train at the different stimulation frequencies. f_2 Plot of the extracellular DC drift measured before each stimulus artifact along the stimulation train. g_1 Sample traces of the antidromic field action potentials, time-locked at the peak during a 24-Hz train. g_2 Plot of the half-width of the antidromic field action potentials along the stimulation train at the different stimulation frequencies. h_1 Sample traces of antidromic field action potentials, time-locked at the stimulation artifact; notice an increasing delay of the antidromic field action potentials onset as stimuli progressed during a 24-Hz train. *Calibration bars* apply to (g_1) and (h_1). h_2 Plot of the time-to-peak of the antidromic field action potentials along the stimulation train at the different stimulation frequencies. All experiments ($n = 5$) were conducted in the presence of glutamatergic antagonists

CA3 pyramidal cells. This was more notorious when the $_f$APs were recorded in the somatic region than when the recordings were conducted over the SC and MF pathways themselves, in which the likelihood of having aborted or inhibited action potentials is low.
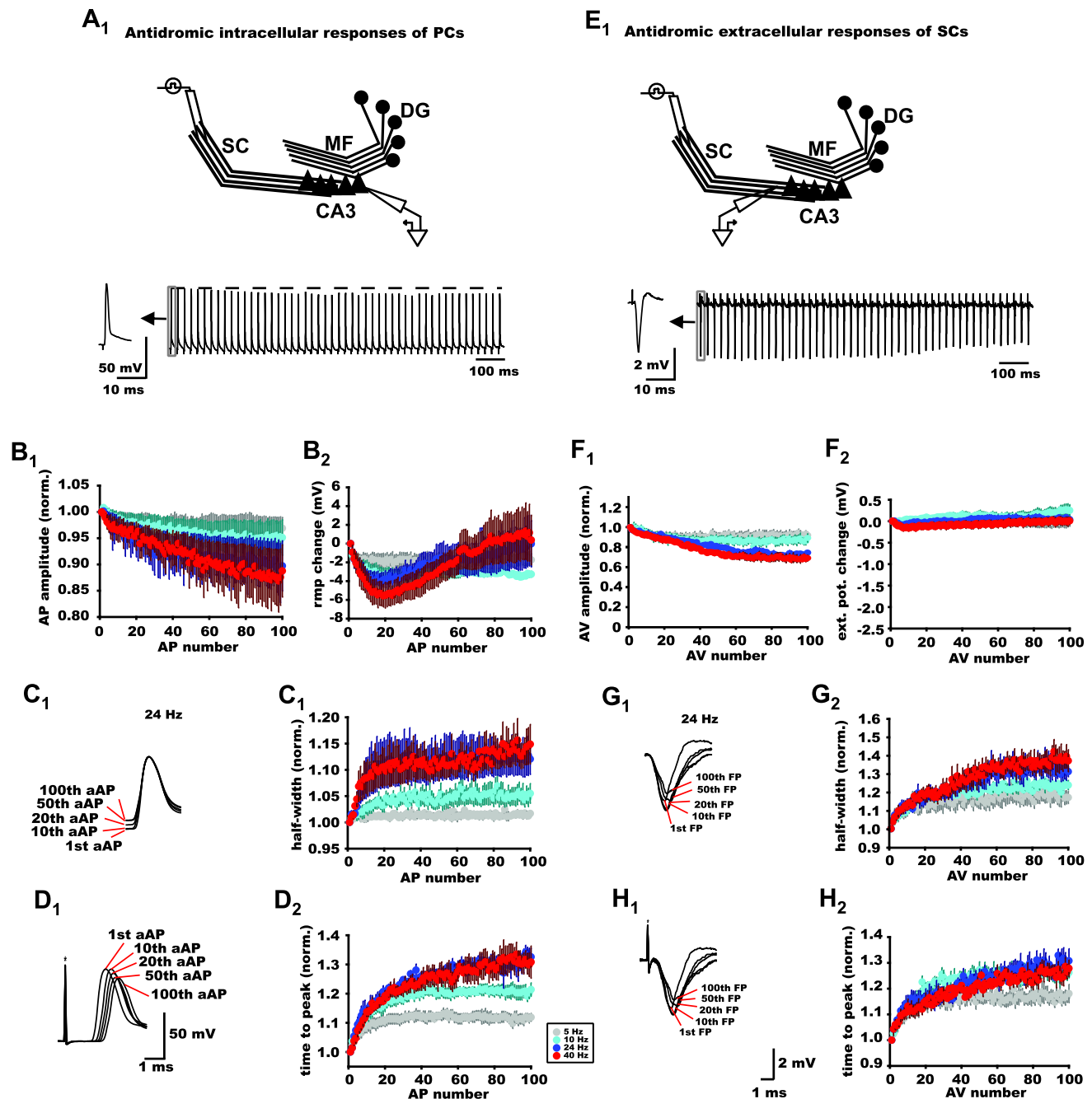
There are a number of differences between the SCs and the MFs that can explain their conduction behavior. The MFs, unlike the SCs, have a tortuous trajectory with giant boutons from which filopodia originate (Claiborne et al. 1986; Ishizuka et al. 1990; Shepherd et al. 2002; Meier et al. 2004), as well as specific characteristics for antidromic conduction, as we here show, probably as a result of distribution of Na^+ channels, ionotropic receptors, geometry differences, and their degree of myelination (Meier et al. 2004; Alle et al. 2009; Sasaki et al. 2011; Ruiz and Kullmann 2013). Importantly, it is known that MFs are endowed with high density of Na^+ channels (Schmidt-Hieber et al. 2008). Moreover, the particular disposition of channels in their boutons (Geiger and Jonas, 2000) and the

communication between their axons by gap junctions may also influence the transit of action potentials along the fibers (Traub et al. 2012). One of the physiological characteristics of MF transmission is that they present robust frequency-dependent potentiation. It is tempting to speculate that the initial potentiation that we uncover by analyzing antidromic potentials can be a reflection of an intrinsic property of conduction that can also be involved in the enhanced release capability of the MF on repetitive stimulation, namely, through activation of Na^+ and K^+ conductances in MF boutons. Moreover, MF boutons can act as sites of amplification of the AP amplitude rather than failure of its propagation. This demonstrates that MFs have highly active properties (Geiger and Jonas 2000; Engel and Jonas 2005).

On the other hand, the decrease of $_f$APs in both pathways along the train may be due to intermittency of firing in certain cells, which we corroborated with intracellular recordings. However, by using a stimulation intensity that evoked action potentials for every stimulus, we observed that the amplitude of both the intracellular and the $_f$APs recorded directly over the axonal tracts was also reduced along the train. We also show, in accordance with other reports, that the half-width (Kim et al. 2012) and latency (Meeks and Mennerick 2007) of the action potentials increased while raising the stimulation frequency; this phenomenon depends on K^+ channel inactivation (Geiger and Jonas 2000), probably mediated by inactivation of Kv1 family (Bean 2007). It is possible that this phenomenon underlies our observation that the action potentials recorded in the granule cells present a hump during high-frequency stimulation, whereas those of pyramidal cells do not.

It is known that high-frequency stimulation promotes extracellular K^+ accumulation. It was interesting that the trend of the response amplitude along the stimulation trains obtained in slices perfused with ACSF containing high-K^+ and low-Ca^{2+} concentrations was similar to the trend obtained under normal ACSF perfusion, although the first responses in each stimulus trains were significantly augmented. This kind of response may also indicate that in our high-frequency stimulation experiments O_2 availability is not compromised (Liotta et al. 2012).

The properties of the antidromically evoked action potentials that we describe can have functional implications in the light of evidence showing that (a) the action potentials of the granule (Schmidt-Hieber et al. 2008) and pyramidal cells (Meeks and Mennerick 2007) are generated in the axons, and (b) axo-axonal electrical coupling occurs in both pathways (Schmitz et al. 2001; Hamzei-Sichani et al. 2007), thus, allowing ectopic action potentials to travel to the soma (Bähner et al. 2011; Dugladze et al. 2012; Traub et al. 2012). Therefore, at high frequencies,

A₁ Antidromic intracellular responses of PCs

E₁ Antidromic extracellular responses of SCs

more cells could be antidromically recruited, probably by facilitation of axo-axonal electrical communication (Traub et al. 2012) resulting in cooperativity that might help to the recruitment of the network (Stacey et al. 2011). Indeed, the changes in conduction velocity in CA3 pyramidal cells (Meeks and Mennerick 2007, present results) may be compensated by axo-axonal electrical cooperativity in both sets of fibers, enabling cell clusters to participate in network activity (Bähner et al. 2011). In any case, repetitive activity shifts the latency of the action potentials arriving to the target cells, which, in turn, need to be able to

"accommodate" this varying entrances into their oscillatory activity (Bean 2007; Bucher and Goaillard 2011; Bukalo et al. 2013). Although in some of our experiments we generate antidromic action potentials that invariably reach the soma, this is not the case under physiological conditions, where ectopically generated action potentials may not (Bähner et al. 2011; Dugladze et al. 2012). Our data reveal that antidromic action potentials electrically evoked in the MFs of slices from control rats make the DG to resonate at a preferred frequency (θ) both in the absence and, to a lesser extent, in the presence of glutamate and

◄ **Fig. 8** Behavior of antidromic potentials evoked by distal SC stimulation and recorded intracellularly in pyramidal cells of CA3 and extracellularly in stratum oriens of CA3. a_1 Schematic representation of the experimental setup. Intracellular recordings were obtained from the pyramidal cells of CA3 and stimulation was provided at different frequencies over the SC. Long time scale and fast time scale sample traces of intracellular recordings of a pyramidal cell showing antidromic action potentials (AP, $n = 100$) on MF stimulation at 5, 10, 24 and 40 Hz. b_1 Plot of the amplitude of the APs along the train at the different stimulation frequencies. b_2 Plot of the RMP measured before each stimulus artifact along the stimulation train. c_1 Sample traces of APs, time-locked at the peak, as stimuli progressed during a 24-Hz train. c_2 Plot of the half-width of the APs along the stimulation train at the different stimulation frequencies. d_1 Sample traces of APs, time-locked at the stimulation artifact; notice an increasing delay of the AP onset as stimuli progressed during a 24-Hz train. d_2 Plot of the time-to-peak of the APs along the stimulation train, at the different stimulation frequencies. *Calibration bars* apply to panels (c_1) and (d_1). e_1 Schematic representation of the experimental setup. Extracellular recordings were obtained from the stratum oriens and stimulation was provided at different frequencies over the stratum radiatum of CA1. Long time scale and fast time scale sample traces of the extracellular recordings of stratum oriens showing antidromic field action potentials (AP, $n = 100$) on SC stimulation at 5, 10, 24 and 40 Hz. f_1 Plot of the amplitude of the antidromic field action potentials along the train at the different stimulation frequencies. f_2 Plot of the extracellular DC drift measured before each stimulus artifact along the stimulation train. g_1 Sample traces of the antidromic field action potentials, time-locked at the peak during a 24-Hz train. g_2 Plot of the half-width of the antidromic field action potentials along the stimulation train at the different stimulation frequencies. h_1 Sample traces of antidromic field action potentials, time-locked at the stimulation artifact, as stimuli progressed during a 24-Hz train. *Calibration bars* apply to panels (g_1) and (h_1). h_2 Plot of the time-to-peak of the antidromic field action potentials along the stimulation train, at the different stimulation frequencies. All experiments were conducted in the presence of glutamatergic antagonists

GABA antagonists, while the opposite occurs in kindled preparations. These results clearly suggest that this phenomenon does not depend on, but can be modulated by tonic activation of ionotropic receptors distributed along the MFs; they could be nonexistent or less active in the SCs (Ruiz and Kullmann 2013). Our data showing that block of glutamate and GABA ionotropic receptors enhances the sustained responses to antidromic stimulation could be interpreted as a reflex of the relaxation of tonic activation, which can underlie axonal noise that can directly modulate synaptic transmission in the MF system (Ruiz and Kullmann 2013; Neishabouri and Faisal 2014). The distal portions of the axons of CA3 pyramidal cells can generate ectopic action potentials at a frequency of 16 Hz during spontaneous gamma frequency activity, whereas the action potentials recorded in the soma reach roughly 4 Hz and the probability of their generation is higher during block of $GABA_A$ receptors. Therefore, $GABA_A$-R-mediated shunting inhibition controls axosomatic coupling, preventing backpropagation of action potentials to the soma (Dugladze et al. 2012).
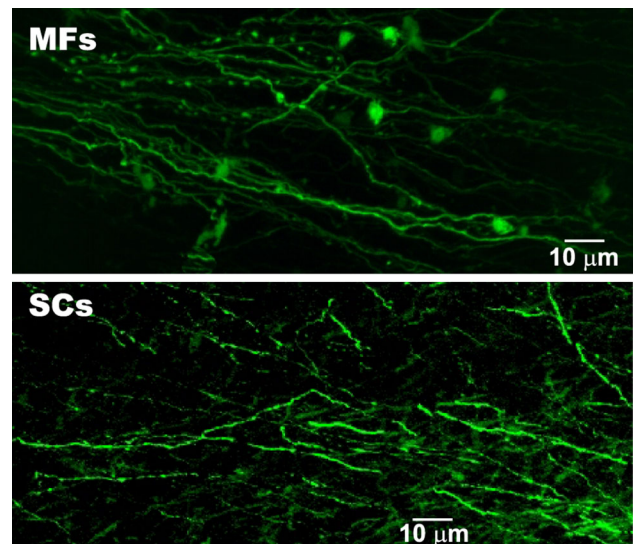

Fig. 9 Confocal images of the mossy fibers and the Schaffer collaterals. The MFs run through a narrow layer (stratum lucidum), where they contact the proximal third of the apical dendrite of the pyramidal cells. Notice the giant boutons and boutons en passant from which filopodial extensions originate. In contrast, the SCs run through the stratum radiatum of CA1 innervating a broader area of the dendritic tree of pyramidal cells. Anatomical and myelination differences, as well as high density of Na^+ channels in the MFs could account for the frequency potentiation of the antidromic responses of this pathway

Interestingly, the $_f$APs recorded in the *strata pyramidale* and *granulare* decrease and increase, respectively, throughout the high-frequency stimulation train, whereas the action potential volleys recorded over the pathways, do so only marginally, suggesting that conductances in the soma can be colliding/counteracting the transmission of the axons. It has been reported that repetitive stimulation (0.2 Hz) of the entorhinal cortex produces neuronal activity in the DG but not in CA3, while stimulation at θ frequency (5 Hz) generates waves of neuronal activity that propagate through the entire hippocampal trisynaptic circuit (Stepan et al. 2012). Moreover, stimulation of the entorhinal cortex at 20 Hz induced a decline of activity in the DG. We disclosed axonal resonance in the DG as a phenomenon which likely contributes to the maintenance and even to the generation of network activity in the hippocampus proper. Both DG and CA3 neurons exhibit intrinsic oscillations at θ frequency, but axonal resonance is subthreshold in CA3, while axonal resonance is suprathreshold in the DG, which helps to drive CA3, as described to happen after short bursts (Henze et al. 2002). Of note is that the presence of resonance in a narrow frequency range could physiologically represent the time window in which the facilitation of the oscillatory activity physiologically occurs. The fact that only one pathway presents resonance speaks in favor of a physiological mechanism that implies

counterbalance. Indeed, there is evidence for minimal interference between signals (Akam and Kullmann 2010) that allows the optimization of information transfer at defined frequencies between CA3 and the DG. It appears that MFs possess a regenerative mechanism that allows them to conduct action potentials at high frequencies and with increased fidelity, whereas the SCs can dampen this forced mechanism imposed upon them in a frequency-dependent manner, even at the low θ frequency band.

The repetitive stimulation that we provided at different frequencies produced an exponential depression of antidromic responses in CA3. We showed that this depression might be due to an increased rate of failures of the fibers to fire action potentials. On the other hand, stimulation applied to the MFs always produced a potentiation in the DG antidromic responses. Altogether, our results show that the increase or decrease of conduction efficacy strongly depends on the pathways that are stimulated as well as on the "receptor" cells somata (see Rosenbaum et al. 2014). These observations can bear clinical implications because deep brain stimulation and transcranial magnetic stimulation have to be provided in a manner in which frequency and number of stimuli provoke a maximal effect to suppress pathological oscillatory activity in the human brain. The hypothesis that a counterbalanced activity in DG and CA3 neurons, in which the amplitude of β and θ oscillations could be modulated via a resonance mechanism, is consistent with recent studies in humans in which the coexistence of both oscillations has been detected. Indeed, Lega et al. (2012) implanted intracranial deep electrodes in hippocampal regions of patients undergoing surgical treatment for intractable epilepsy and obtained electrical recordings while participants studied and recalled a list of words in a delayed free-recall task. The power spectra of these recordings exhibited two dominant peaks, one in the θ and other in the β/γ frequency band, suggesting that both rhythms coexist in the human hippocampus. Because the amplitude of these dominant peaks was different among different subjects and trials, in some cases, the θ was bigger than β, or vice versa, it is tempting to speculate that a counterbalanced activity of DG and CA3 neurons via resonance mechanisms is involved in such diversity of β and θ peak amplitudes. Finally, this suggests that resonance effects may be involved in the balance of excitation and inhibition of stimulated structures, especially if stimulation is provided to fiber tracts to activate their origin antidromically, which, by itself, can induce a type of postsynaptic cell-dependent plasticity (Bukalo et al. 2013).

References

Akam T, Kullmann DM (2010) Oscillations and filtering networks support flexible routing of information. Neuron 67:308–320

Akam T, Oren I, Mantoan L, Ferenczi E, Kullmann DM (2012) Oscillatory dynamics in the hippocampus support dentate gyrus-CA3 coupling. Nat Neurosci 15:763–768

Alle H, Roth A, Geiger JR (2009) Energy-efficient action potentials in hippocampal mossy fibers. Science 325:1405–1408

Bähner F, Weiss EK, Birke G, Maier N, Schmitz D, Rudolph U, Frotscher M, Traub RD, Both M, Draguhn A (2011) Cellular correlate of assembly formation in oscillating hippocampal networks in vitro. Proc Natl Acad Sci USA 108:607–616

Bean BP (2007) The action potential in mammalian central neurons. Nat Rev Neurosci 8:451–465

Berke JD, Hetrick V, Breck J, Greene RW (2008) Transient 23–30 Hz oscillations in mouse hippocampus during exploration of novel environments. Hippocampus 18:519–529

Boulton CL, von Haebler D, Heinemann U (1992) Tracing of axonal connections by rhodamine–dextran-amine in the rat hippocampal–entorhinal cortex slice preparation. Hippocampus 2:99–106

Bower MR, Buckmaster PS (2008) Changes in granule cell firing rates precede locally recorded spontaneous seizures by minutes in an animal model of temporal lobe epilepsy. J Neurophysiol 99:2431–2442

Bucher D, Goaillard JM (2011) Beyond faithful conduction: short-term dynamics, neuromodulation, and long-term regulation of spike propagation in the axon. Prog Neurobiol 94:307–346

Bukalo O, Campanac E, Hoffman DA, Fields RD (2013) Synaptic plasticity by antidromic firing during hippocampal network oscillations. Proc Natl Acad Sci USA 110:5175–5180

Claiborne BJ, Amaral DG, Cowan WM (1986) A light and electron microscopic analysis of the MFs of the rat dentate gyrus. J Comp Neurol 246:435–458

Dugladze T, Schmitz D, Whittington MA, Vida I, Gloveli T (2012) Segregation of axonal and somatic activity during fast network oscillations. Science 336:1458–1461

Engel D, Jonas P (2005) Presynaptic action potential amplification by voltage-gated Na+ channels in hippocampal mossy fiber boutons. Neuron 45:405–417

Geiger JR, Jonas P (2000) Dynamic control of presynaptic Ca(2+) inflow by fast-inactivating K(+) channels in hippocampal mossy fiber boutons. Neuron 28:927–939

Gutiérrez R (2000) Seizures induce simultaneous GABAergic and glutamatergic neurotransmission in the dentate gyrus—CA3 system. J Neurophysiol 84:3088–3090

Hamzei-Sichani F, Kamasawa N, Janssen WGM, Yasamura T, Davidson KGV, Hof PR, Wearne SL, Stewart MG, Young SR, Whittington MA, Rash JE, Traub RD (2007) Gap junctions on hippocampal mossy fiber axons demonstrated by thin-section electron microscopy and freeze-fracture replica immunogold labeling. Proc Natl Acad Sci USA 104:12548–12553

Henze DA, Wittner L, Buzsáki G (2002) Single granule cells reliably discharge targets in the hippocampal CA3 network in vivo. Nat Neurosci 5:790–795

Ishizuka N, Weber J, Amaral DG (1990) Organization of intrahippocampal projections originating from CA3 pyramidal cells in the rat. J Comp Neurol 295:580–623

Jaffe DB, Gutiérrez R (2007) Mossy fiber synaptic transmission: communication from the dentate gyrus to area CA3. Prog Brain Res 163:109–805

Jung MW, McNaughton BL (1993) Spatial selectivity of unit activity in the hippocampal granular layer. Hippocampus 3:165–182

Kim E, Owen B, Holmes WR, Grover LM (2012) Decreased afferent excitability contributes to synaptic depression during high frequency stimulation in hippocampal area CA1. J Neurophysiol 108:1965–1976

Lega BC, Jacobs J, Kahana M (2012) Human hippocampal theta oscillations and the formation of episodic memories. Hippocampus 22:748–761

Liotta A, Rösner J, Huchzermeyer C, Wojtowicz A, Kann O, Schmitz D, Heinemann U, Kovács R (2012) Energy demand of synaptic transmission at the hippocampal Schaffer-collateral synapse. J Cereb Blood Flow Metab 32:2076–2083

Manjarrez E, Rojas-Piloni G, Méndez I, Flores A (2003) Stochastic resonance within the somatosensory system: effects of noise on evoked field potentials elicited by tactile stimuli. J Neurosci 23:1997–2001

Meeks JP, Mennerick S (2007) Action potential initiation and propagation in CA3 pyramidal axons. J Neurophysiol 97:3460–3472

Meier S, Bräuer AU, Heimrich B, Nitsch R, Savaskan NE (2004) Myelination in the hippocampus during development and following lesion. Cell Mol Life Sci 61:1082–1094

Neishabouri A, Faisal AA (2014) Axonal noise as a source of synaptic variability. PLoS Comput Biol 10:e1003615

Pietersen AN, Patel N, Jefferys JGR, Vreugdenhil M (2009) Comparison between spontaneous and kainate-induced gamma oscillations in the mouse hippocampus in vitro. Eur J Neurosci 2145–2156

Roopun AK, Middleton SJ, Cunningham MO, LeBeau FE, Bibbig A, Whittington MA, Traub RD (2006) A beta2-frequency (20–30 Hz) oscillation in nonsynaptic networks of somatosensory cortex. Proc Natl Acad Sci USA 103:15646–15650

Rosenbaum R, Zimnikc A, Zheng F, Turner RS, Alzheimer C, Doiron B, Rubina JE (2014) Axonal and synaptic failure suppress the transfer of firing rate oscillations, synchrony and information during high frequency deep brain stimulation. Neurobiol Dis 62:86–99

Ruiz AJ, Kullmann DM (2013) Ionotropic receptors at hippocampal mossy fibers: roles in axonal excitability, synaptic transmission, and plasticity. Front Neural Circuits 6:112

Sasaki T, Matsuki N, Ikegaya Y (2011) Action-potential modulation during axonal conduction. Science 331:599–601

Schmidt-Hieber C, Jonas P, Bischofberger J (2008) Action potential initiation and propagation in hippocampal mossy fibre axons. J Physiol 586(7):1849–1857

Schmitz D, Schuchmann S, Fisahn A, Draguhn A, Buhl EH, Petrasch-Parwez RE, Dermietzel R, Heinemann U, Traub RD (2001) Axo-axonal coupling: a novel mechanism for ultrafast neuronal communication. Neuron 31:831–840

Shepherd MG, Raastad M, Andersen P (2002) General and variable features of varicosity spacing along unmyelinated axons in the hippocampus and cerebellum. Proc Natl Acad Sci USA 99:6340–6345

Shimono K, Brucher F, Granger R, Lynch G, Taketani M (2000) Origins and distribution of cholinergically induced β rhythms in hippocampal slices. J Neurosci 20:8462–8473

Stacey WC, Krieger A, Litt B (2011) Network recruitment to coherent oscillations in a hippocampal computer model. J Neurophysiol 105:1464–1481

Stepan J, Dine J, Fenz T, Polta SA, vonWolff G, Wotjak CT, Eder M (2012) Entorhinal theta-frequency input to the dentate gyrus trisynaptically evokes hippocampal CA1 LTP. Front Neural Circuits 6:Art. 64

Traub RD, Schmitz D, Maier N, Whittington MA, Draguhn A (2012) Axonal properties determine somatic firing in a model of in vitro CA1 hippocampal sharp wave/ripples and persistent gamma oscillations. Eur J Neurosci 36:2650–2660

Treviño M, Vivar C, Gutiérrez R (2007) β/γ Oscillatory activity in the CA3 hippocampal area is depressed by aberrant GABAergic transmission from the dentate gyrus after seizures. J Neurosci 27:251–259

Treviño M, Vivar C, Gutiérrez R (2011) Excitation-inhibition balance in the CA3 network—neuronal specificity and activity-dependent plasticity. Eur J Neurosci 33:1771–1785